Alexandria Engineering Journal (2023) 71, 401–411

HOSTED BY

Alexandria University

Alexandria Engineering Journal

www.elsevier.com/locate/aej
www.sciencedirect.com

ORIGINAL ARTICLE

Dual solutions on MHD radiative three-dimensional bidirectional nanofluid flow over a non-linearly permeable shrinking sheet

Najiyah Safwa Khashi'ie [a,b], **Natalia C. Roşca** [c], **Alin V. Roşca** [d], **Ioan Pop** [c,*]

[a] *Fakulti Teknologi Kejuruteraan Mekanikal dan Pembuatan, Universiti Teknikal Malaysia Melaka, 76100 Durian Tunggal, Malaysia*
[b] *Forecasting and Engineering Technology Analysis (FETA) Research Group, Universiti Teknikal Malaysia Melaka, 76100 Durian Tunggal, Malaysia*
[c] *Faculty of Mathematics and Computer Science, Department of Mathematics, Babeş-Bolyai University, 400084 Cluj-Napoca, Romania*
[d] *Faculty of Economics and Business Administration, Department of Statistics-Forecasts-Mathematics, Babeş-Bolyai University, 400084 Cluj-Napoca, Romania*

Received 21 February 2023; revised 18 March 2023; accepted 21 March 2023

KEYWORDS

Dual solutions;
Magnetohydrodynamics;
Nanofluid;
Nonlinear shrinking;
Thermal radiation

Abstract The bidirectional flow and thermal transfer of magnetohydrodynamics (MHD) and radiative nanofluid (magnetite-vacuum pump oil) due to a nonlinear shrinking surface in a three dimensional system is studied. The boundary layer model is first transformed into a set of ordinary differential equations using the similarity transformations, and then solved using the bvp4c solver. The accuracy of the present model is justified by comparing present data with the numerical values from the published findings. The effect of factors (magnetic parameter, radiation parameter and nanoparticles volumetric concentration) on the development of responses (skin friction coefficient and thermal rate) and critical value (separation value from laminar to turbulent flow) is observed through the graphical presentation. In addition, two solutions are attained where the first solution is affirmed as the reliable solution through stability analysis. Conclusively, the suction effect is necessary in generating the solutions under the phenomenon of opposing shrinking flow. The addition of magnetic parameter and nanoparticles concentration can enhance both responses as well as the critical value while the radiation parameter tends to reduce the heat transfer coefficient. The types of stretching/shrinking velocity (linear/nonlinear) also affect the heat transfer rate. The critical value can be extended by using the linear velocity, but, for thermal enhancement, the nonlinear form of velocity can significantly develop the thermal rate better than the linear shrinking surface.

* Corresponding author.
E-mail address: popm.ioan@yahoo.co.uk (I. Pop).
Peer review under responsibility of Faculty of Engineering, Alexandria University.

https://doi.org/10.1016/j.aej.2023.03.066
1110-0168 © 2023 THE AUTHORS. Published by Elsevier BV on behalf of Faculty of Engineering, Alexandria University.
This is an open access article under the CC BY-NC-ND license (http://creativecommons.org/licenses/by-nc-nd/4.0/).

1. Introduction

Heat transfer improvement has drawn the attention of numerous academic and industrial researchers for many years. Due to its numerous practical applications in chemical processes and modern manufacturing like solar physics, metallurgy, cosmic fluid dynamics, geophysics, earth's core motion, the polymer industry, etc., magnetohydrodynamic (MHD) effects have attracted considerable attention from researchers over the past few decades. The magnetohydrodynamic effects have been used in a sizable number of studies for their investigation. The influence of MHD on heat transfer in a vertical permeable plate has been studied, as well as flows in stagnation point flows with magnetohydrodynamic and slip effect. A similar effect of magnetohydrodynamic for the case of nonlinear extending sheet with the addition of viscous dissipation effect has also been studied. The induced flow across a surface that is extending or contracting is a very well-known problem in fluid mechanics. It usually occurs during the the extrusion of polymer sheets from dies, the fabrication of paper and glass fibre, the cooling of metallic plates in a bath, and many other processes. Researchers have become interested in this flow problem with heat transfer because it has applications in polymer processing technology. Both of the stretching and cooling speeds have an impact on the final product's quality in the industrial setting. There is a sizable body of literature on this subject.

Maxwell [1] took the initiative to work on improving the fluid's thermal conductivity. However, there were just a few problems with fluid stability and rheology [2]. The heat transfer fluid was enhanced by Choi and Eastman [3] by scattering the nanoparticles. Since then, much research and explanations have been made about the stability, thermal conductivity, and synthesis of nanofluids [4–8]. The most common nanoparticles fall into the following categories: metal oxides (i.e ferric oxide/Fe_2O_3, aluminium oxide/Al_2O_3), metals (i.e silver/Ag, copper/Cu, nickel/Ni), carbon materials, metal carbide and metal nitride. On the other hand, the basic fluids which frequently utilized to create nanofluids are often water, ethylene glycol, and engine oil. Ferrofluids, or magnetic nanofluids, are ion-based nanoparticles like magnetite (Fe_3O_4), cobalt ferrite ($CoFe_2O_4$), hematite (Fe_2O_3) and manganese-zinc ferrite ($Mn\text{-}ZnFe_2O_4$). Ferrofluid has a potential uses in the biomedical field, including drug administration, cancer treatment, and MRI [9,10]. The applications of magnetic nanofluids were discussed by Bahiraei and Hangi [11] specifically in thermal management systems. The magnetic characteristics of soft ferrite like $Mn\text{-}ZnFe_2O_4$ in applications related to high frequency transformer were highlighted by Petrescu et al. [12].

In industrial processes like the fabrication of glass fibre, the extrusion of polymers, and crystal growth, this kind of study reveals an upward trend and enduring needs due to its importance [13–15]. There are two well-known models which are often used by researchers to forecast how nanofluids will flow (see two phase model/Buongiorno [16] and single phase model/Tiwari and Das [17]). Jusoh et al. [18] studied three different base fluids; water, kerosene, and methanol while Ahmed et al. [19] examined the MNFs flow towards a wedge using $Mn\text{-}ZnFe_2O_4\text{-}H_2O$ (manganese-zinc ferrite-water) and $CoFe_2O_4\text{-}H_2O$ (cobalt ferrite-water) nanofluids. The magnetite nanofluid motion with homogeneous-heterogeneous reactions was studied by Hayat et al [20]. The stagnation point flow of a magnetite-water towards a stretched sheet was analyzed by Mohamed et al. [21] in relation to the effects of MHD, slip effect and Newtonian heating. Using magnetite and SWCNT nanoparticles, Areekara et al. [22] highlighted the combined impacts of stratification, chemical reaction, viscous dissipation and generated magnetic field for the stagnation point flow of nanofluid. Very recent, Khashi'ie et al. [23] discussed the comparative analysis between manganese-zinc-water, cobalt ferrite-water, magnetite-water flow over a shrinking sheet with few physical effects. They revealed that the manganese-zinc-water has the largest thermal coefficient. They also found the significance of Fe_3O_4-water in the expansion of critical value better than other tested MNFs. Many intriguing articles about the heat transfer and movement of nanofluids in two and three dimensional system (boundary layer flow) can be found here [24–35] as well as in Khan [36,37], Lanjwani et al. [38,39] and Khan et al. [40]. It is worth mentioning that many references on nanofluids can be found in the books by Das et al. [41], Nield and Bejan [42], Shenoy et al. [43] and Merkin et al. [44].

Therefore, being motivated by the difference behaviours of nanofluids thermal progress and flow under different circumstances, this study will analyse the three-dimensional, bidirectional flow and thermal characteristics of radiated magnetic nanofluid (magnetite) with vacuum pump oil as the base fluid over a shrinking surface. Three issues about the flow and heat transfer characteristics of the nanofluids are raised:

- Is the non-unique solutions for the magnetite-VPO bidirectional flow under the simultaneous effects of shrinking surface, MHD and radiation can be generated if no suction is imposed?
- Does the increasing values of magnetic parameter, thermal radiation and nanoparticles concentration significantly affect the flow, heat transfer and boundary layer separation?
- Which case of the shrinking surface (linear/nonlinear) extends the separation value and produce the highest thermal rate?

The research questions listed above will be addressed by the findings in Section 5. In the procedure, the governing model is simplified using the similarity transformation approach, and the numerical calculation is handled by the bvp4c solver. The authors are affirm that the current work can have a substantial influence and provide other researchers with suggestions for choosing an appropriate host fluid and physical parameter for the thermal and flow advancement in contemporary industry.

2. Mathematical formulation

The MHD three-dimensional bidirectional nanofluid (ferro (Fe_3O_4)− vacuum pump oil (VPO)) motion over a nonlinear shrinking sheet is considered, as shown in Fig. 1, where the flow occupies the domain $z \geq 0$. It is assumed that the shrinking velocities in the $(x, y)-$directions are $U_w(x, y) = u_w(x, y)\lambda = a(x+y)^n\lambda$ and $V_w(x, y) = v_w(x, y)\lambda = a(x+y)^n\lambda$, where $a > 0$ and n is the nonlinear parameter where $n > 1$ denotes the nonlinear shrinking velocity and $n = 1$ implies the linear

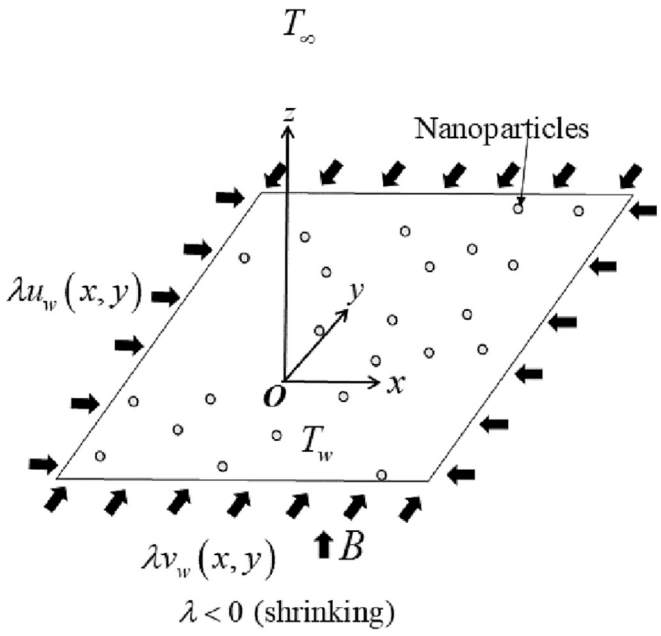

Fig. 1 The physical model.

case . Further, $\lambda < 0$ is the constant shrinking parameter and w_w is the mass flux velocity with $w_w(x,y) < 0$ for suction. The variable magnetic field $B = B_0(x+y)^{(n-1)/2}$ is applied in the direction of $z-$ axis, with B_0 being the constant strength magnetic, and the heat radiation effect q_r are considered in the current analysis. It is also assumed that the viscous dissipation and Joule heating are ignored. The constant temperature of the surface is T_w, while T_∞ represents the free stream temperature. For the magnetic field expression, the electric field is excluded by considering that no voltage is applied to the fluid motion. Hence, the current density vector $\mathbf{J}$ is given by (see Shercliff [45])

$$\mathbf{J} = \sigma_{nf}(\mathbf{V} \times \mathbf{B}) \times \mathrm{B} \tag{1}$$

where $\mathbf{J} = (J_x, J_y, J_z)$ and the magnetic induction is $\mathbf{B}(0,0,B_0)$. So, $\mathbf{J}$ is, in components form, given by (see Shercliff [45])

$$J_x = -\sigma_{nf}B^2u, J_y = -\sigma_{nf}B^2v \tag{2}$$

Under these assumptions, the suitable model of nanofluid can be written as (see Jusoh et al. [18], Khashi'ie et al. [23], Ramzan et al. [29]):

$$\frac{\partial u}{\partial x} + \frac{\partial v}{\partial y} + \frac{\partial w}{\partial z} = 0, \tag{3}$$

$$u\frac{\partial u}{\partial x} + v\frac{\partial u}{\partial y} + w\frac{\partial u}{\partial z} = \frac{\mu_{nf}}{\rho_{nf}}\frac{\partial^2 u}{\partial z^2} - \frac{\sigma_{nf}B^2}{\rho_{nf}}u, \tag{4}$$

$$u\frac{\partial v}{\partial x} + v\frac{\partial v}{\partial y} + w\frac{\partial v}{\partial z} = \frac{\mu_{nf}}{\rho_{nf}}\frac{\partial^2 v}{\partial z^2} - \frac{\sigma_{nf}B^2}{\rho_{nf}}v, \tag{5}$$

$$u\frac{\partial T}{\partial x} + v\frac{\partial T}{\partial y} + w\frac{\partial T}{\partial z} = \frac{k_{nf}}{(\rho C_p)_{nf}}\frac{\partial^2 T}{\partial z^2} - \frac{1}{(\rho C_p)_{nf}}\frac{\partial q_r}{\partial z}, \tag{6}$$

subject to the boundary conditions (see Ramzan et al. [29])

$$\left.\begin{array}{c} u(x,y,0) = \lambda u_w(x,y) = \lambda a(x+y)^n,\ v(x,y,0) = \lambda u_w(x,y) = \lambda a(x+y)^n, \\ w(x,y,0) = w_w,\ T(x,y,0) = T_w, \end{array}\right\} \tag{7}$$

$$u(x,y,z) \to 0,\ v(x,y,z) \to 0,\ T(x,y,z) \to T_\infty \text{ as } z \to \infty \tag{8}$$

Here (u,v,w) are the velocity components of the nanofluid along (x,y,z) axis and T is the temperatures of the nanofluid. Further, μ_{nf} is the dynamic viscosity, ρ_{nf} is the density, k_{nf} is the thermal conductivity, $(\rho C_p)_{nf}$ is the heat capacity and σ_{nf} is the electrical conductivity of the nanofluid, which are given by (see Table 1).

where ϕ is the volume fraction of nanofluid with $\phi = 0$ corresponding to a regular fluid, μ_f is dynamic viscosity, ρ_f and ρ_s are densities, $k_f$andk_s are thermal diffusivities, $(\rho C_p)_f$ and $(\rho C_p)_s$ are the heat capacities of the base fluid and nanoparticles, σ is the effective electrical conductivity and C_p is the heat capacity at a constant pressure. Meanwhile, the properties for the present base fluid and nanoparticle are provided in Table 2 (see Ramzan et al. [29]).

In Table 2, R is the electrical resistance of a sample of material of length L and uniform cross- sectional area S. For the thermal radiation approximation based on Cortell [46], the radiative heat flux q_r is

Table 1 Correlations of a general nanofluid.

Properties	Correlations
Thermal conductivity	$k_{nf} = \frac{k_s+2k_f-2\phi(k_f-k_s)}{k_s+2k_f+\phi(k_f-k_s)}k_f$
Electrical conductivity	$\sigma_{nf} = \left[1 + \frac{3(\sigma-1)\phi}{(\sigma+2)-(\sigma-1)\phi}\right]\sigma_f;\ \sigma = \frac{\sigma_s}{\sigma_f}$
Heat capacity	$(\rho C_p)_{nf} = (1-\phi)(\rho C_p)_f + \phi(\rho C_p)_s$
Density	$\rho_{nf} = (1-\phi)\rho_f + \phi\rho_s$
Dynamic viscosity	$\mu_{nf} = \frac{1}{(1-\phi)^{2.5}}\mu_f$

Table 2 Properties of vacuum pump oil (VPO) and magnetite nanoparticle.

Properties	Magnetite	Vacuum pump oil (VPO)
$\rho(\mathrm{kg/m^3})$	5180	870
$C_p(\mathrm{J/kgK})$	670	2320
$k(\mathrm{W/mK})$	80	0.13
$\mu(\mathrm{kg/m^3})$	10^{-6}	93.1
$\sigma(L/RS)$	2.99×10^{-3}	56.6

$$q_r = -\frac{4\sigma^*}{3k^*}\frac{\partial T^4}{\partial y}. \tag{9}$$

Following Rosseland [47], the term T^4 in Eq. (9) is simplified to $T^4 \approx 4\,T_\infty^3 T - 3T_\infty^4$ and simultaneously transform Eq. (6) into

$$u\frac{\partial T}{\partial x} + v\frac{\partial T}{\partial y} + w\frac{\partial T}{\partial z} = \frac{1}{(\rho C_p)_{nf}}\left[k_{nf} + \frac{16\sigma^* T_\infty^3}{3k^*}\right]\frac{\partial^2 T}{\partial z^2}. \tag{10}$$

As in Ramzan et al. [29], it is suitable to introduce the following similarity variables

$$\left.\begin{aligned} u = a(x+y)^n f'(\eta), w = -\sqrt{\tfrac{n+1}{2}av_f}(x+y)^{\frac{n-1}{2}}[f(\eta) + g(\eta) + \tfrac{n-1}{n+1}\eta(f'(\eta)+g'(\eta))], \\ v = b(x+y)^n g'(\eta), \eta = \sqrt{\tfrac{n+1}{2}\tfrac{a}{v_f}}(x+y)^{\frac{n-1}{2}} z, \theta(\eta) = \tfrac{T-T_\infty}{T_w - T_\infty}. \end{aligned}\right\} \tag{11}$$

Thus, the mass flow velocity for the permeable surface is formulated as

$$w_w = -\sqrt{\frac{2}{n+1}av_f}(x+y)^{\frac{n-1}{2}} S, \tag{12}$$

where $S = g(0), f(0) = 0$ is the constant mass flux velocity with $S > 0$ for suction and $S < 0$ for injection, respectively. Substituting (11) into Eqs. (3) to (6), we obtain the following ordinary (similarity) differential equations (see Khashi'ie et al. [23,26], Ramzan et al. [29])

$$\left(\frac{\mu_{nf}/\mu_f}{\rho_{nf}/\rho_f}\right)f''' + (f+g)f'' - \frac{2n}{n+1}(f'+g')f' - \frac{2n}{n+1}\frac{\sigma_{nf}/\sigma_f}{\rho_{nf}/\rho_f}Mf' = 0 \tag{13}$$

$$\left(\frac{\mu_{nf}/\mu_f}{\rho_{nf}/\rho_f}\right)g''' + (f+g)g'' - \frac{2n}{n+1}(f'+g')g' - \frac{2n}{n+1}\frac{\sigma_{nf}/\sigma_f}{\rho_{nf}/\rho_f}Mg' = 0 \tag{14}$$

$$\frac{1}{\mathrm{Pr}\left((\rho C_p)_{nf}/(\rho C_p)_f\right)}\left(\frac{k_{nf}}{k_f} + \frac{4}{3}R\right)\theta'' + (f+g)\theta' = 0, \tag{15}$$

subject to the boundary conditions:

$$\begin{aligned} &f(0) = S,\ g(0) = 0, f'(0) = g'(0) = \lambda,\ \theta(0) = 1, \\ &f'(\eta) \to 0,\ g'(\eta) \to 0, \theta(\eta) \to 0,\ as\ \eta \to \infty \end{aligned} \tag{16}$$

where, $\mathrm{Pr} = (C_p\mu)_f/k_f$ is the Prandtl number, $M = \sigma_f B_0^2/a\rho_f$ is the magnetic parameter and $R = 4\sigma^*\,T_\infty^3/k_f k^*$ is the radiation parameter. In addition, the quantities of the practical interest are the skin friction coefficients C_{fx} and C_{fy}, and the local Nusselt number Nu_x, which are defined as (see Khashi'ie et al. [23,26], Ramzan et al. [29])

$$\begin{aligned} &C_{fx} = \frac{\mu_{nf}\left(\frac{\partial u}{\partial z}\right)_{z=0}}{(x+y)\rho_f u_w^2}, C_{fy} = \frac{\mu_{nf}\left(\frac{\partial v}{\partial z}\right)_{z=0}}{(x+y)\rho_f v_w^2}, \\ &Nu_x = -\frac{(x+y)k_{nf}}{k_f(T_w - T_\infty)}\left(\frac{\partial T}{\partial z}\right)_{z=0} + (x+y)(q_r)_{z=0} \end{aligned} \tag{17}$$

Using (11) and (17),

$$\left.\begin{aligned} Re_x^{1/2}C_{fx} = \sqrt{\tfrac{n+1}{2}}\tfrac{\mu_{nf}}{\mu_f}f''(0), Re_y^{1/2}C_{fy} = \sqrt{\tfrac{n+1}{2}}\tfrac{\mu_{nf}}{\mu_f}g''(0), \\ Re_x^{-1/2}Nu_x = -\left(\tfrac{k_{nf}}{k_f} + \tfrac{4}{3}R\right)\theta'(0) \end{aligned}\right\} \tag{18}$$

where $Re_x = u_w(x+y)/v_f$ and $Re_y = v_w(x+y)/v_f$ are the local Reynolds numbers along $x-$ and $y-$ directions, respectively.

3. Special cases

3.1. Exact analytical solutions for the two-dimensional flow and heat transfer problem with $\boldsymbol{g(\eta) = 0}$ $\boldsymbol{n = 1}$ and $\boldsymbol{R = 0}$.

For this special case, Eqs. (13) and (15) along with the boundary conditions (16) are reduced to

$$\left(\frac{\mu_{nf}/\mu_f}{\rho_{nf}/\rho_f}\right)f''' + ff'' - f'^2 - \frac{\sigma_{nf}/\sigma_f}{\rho_{nf}/\rho_f}Mf' = 0 \tag{19}$$

$$\frac{1}{\mathrm{Pr}}\left(\frac{k_{nf}/k_f}{(\rho C_p)_{nf}/(\rho C_p)_f}\right)\theta'' + f\theta' = 0, \tag{20}$$

subject to the boundary conditions:

$$\begin{aligned} &f(0) = S,\ f'(0) = \lambda,\ \theta(0) = 1, \\ &f'(\eta) \to 0,\ \theta(\eta) \to 0,\ \text{as}\ \eta \to \infty \end{aligned} \tag{21}$$

The closed form analytical solution of this boundary value problem is given as (see Govindaraju et al. [48])

$$f(\eta) = S - \frac{\lambda}{\alpha_2}(1 - e^{-\alpha_2\eta}) \tag{22}$$

where α_2 is given by

$$\alpha_2 = \frac{1}{2\left(\frac{\mu_{nf}/\mu_f}{\rho_{nf}/\rho_f}\right)}\left\{S + \sqrt{S^2 + 4\left[\lambda + \frac{\sigma_{nf}/\sigma_f}{\rho_{nf}/\rho_f}M\right]}\right\} \tag{23}$$

3.2. Two-dimensional flow for $\boldsymbol{\phi = 0}, \boldsymbol{n = 1}$ and $\boldsymbol{M = R = 0}$ and $\boldsymbol{\lambda = -1}$.

For this special case, Eqs. (13) and (15) along with the boundary conditions (16) are reduced to

$$f''' + ff'' - f'^2 = 0 \tag{24}$$

subject to the boundary conditions:

$$\begin{aligned} &f(0) = S,\ f'(0) = -1, \\ &f'(\eta) \to 0,\ \text{as}\ \eta \to \infty \end{aligned} \tag{25}$$

reduces to the expression discussed by Miklavčič and Wang [49], namely

$$f(\eta) = C + \frac{1}{C}e^{-\eta}; S = C + \frac{1}{C} \tag{26}$$

where C is a constant.

4. Stability analysis

This analysis has been a routine procedure for the generation of multiple solutions. Based on the stability analysis, the first solution which initially fulfil the boundary condition is always validated as the reliable and stable solution. However, there were also cases where more than one stable solution exist (see Waini et al. [50] and Khashi'ie et al. [51]). Hence, it is crucial to check the stability of each solution(s). Following Merkin [52], the following transformation is considered for the unsteady problem of Eqs. (3)-(6):

$$u = a(x+y)^n \frac{\partial f(\eta,\tau)}{\partial \eta},\ v = b(x+y)^n \frac{\partial g(\eta,\tau)}{\partial \eta},\ \eta = \sqrt{\frac{n+1}{2}\frac{a}{\nu_f}}(x+y)^{\frac{n-1}{2}}z,$$
$$w = -\sqrt{\frac{n+1}{2}a\nu_f}(x+y)^{\frac{n-1}{2}}\left[f(\eta,\tau) + g(\eta,\tau) + \frac{n-1}{n+1}\eta\left(\frac{\partial f(\eta,\tau)}{\partial \eta} + \frac{\partial g(\eta,\tau)}{\partial \eta}\right)\right],$$
$$\tau = a(x+y)^{n-1}t \text{ (time variable)},\ \theta(\eta,\tau) = \frac{T-T_\infty}{T_w - T_\infty}. \tag{27}$$

The transformed differential equations after considering time variable transformation in Eq. (27) into the unsteady problem of Eqs. (3)-(6) are

$$\left(\frac{\mu_{nf}/\mu_f}{\rho_{nf}/\rho_f}\right)\frac{\partial^3 f}{\partial \eta^3} + (f+g)\frac{\partial^2 f}{\partial \eta^2} - \frac{2n}{n+1}\left(\frac{\partial f}{\partial \eta} + \frac{\partial g}{\partial \eta}\right)\frac{\partial f}{\partial \eta}$$
$$-\frac{2n}{n+1}\left(\frac{\sigma_{nf}/\sigma_f}{\rho_{nf}/\rho_f}M\frac{\partial f}{\partial \eta} + \frac{\partial^2 f}{\partial \eta \partial \tau}\right) = 0 \tag{28}$$

$$\left(\frac{\mu_{nf}/\mu_f}{\rho_{nf}/\rho_f}\right)\frac{\partial^3 g}{\partial \eta^3} + (f+g)\frac{\partial^2 g}{\partial \eta^2} - \frac{2n}{n+1}\left(\frac{\partial f}{\partial \eta} + \frac{\partial g}{\partial \eta}\right)\frac{\partial g}{\partial \eta}$$
$$-\frac{2n}{n+1}\left(\frac{\sigma_{nf}/\sigma_f}{\rho_{nf}/\rho_f}M\frac{\partial g}{\partial \eta} + \frac{\partial^2 g}{\partial \eta \partial \tau}\right) = 0 \tag{29}$$

$$\frac{1}{\Pr\left(\left(\rho C_p\right)_{nf}/\left(\rho C_p\right)_f\right)}\left(\frac{k_{nf}}{k_f} + \frac{4}{3}R\right)\frac{\partial^2 \theta}{\partial \eta^2} + (f+g)\frac{\partial \theta}{\partial \eta}$$
$$-\frac{2}{n+1}\frac{\partial \theta}{\partial \tau} = 0, \tag{30}$$

subject to the boundary conditions

$$f(0,\tau) = S,\ g(0,\tau) = 0,\ \frac{\partial f(0,\tau)}{\partial \eta} = \lambda,\ \frac{\partial g(0,\tau)}{\partial \eta} = \lambda,\ \theta(0,\tau) = 1,$$
$$\frac{\partial f(\eta,\tau)}{\partial \eta} \to 0,\ \frac{\partial g(\eta,\tau)}{\partial \eta} \to 0,\ \theta(\eta,\tau) \to 0,\ \text{as } \eta \to \infty. \tag{31}$$

The purpose of the perturbation function is to examine any potential disruption in the solutions (see Weidman et al. [53]) such that:

$$f(\eta,\tau) = f_0(\eta) + e^{-\gamma\tau}F_0(\eta,\tau),$$
$$g(\eta,\tau) = g_0(\eta) + e^{-\gamma\tau}G_0(\eta,\tau), \tag{32}$$
$$\theta(\eta,\tau) = \theta_0(\eta) + e^{-\gamma\tau}H_0(\eta,\tau)$$

By inserting Eq. (32) into Eqs. (28)-(30), the linearized eigenvalue equations are produced such that:

$$\frac{\mu_{nf}/\mu_f}{\rho_{nf}/\rho_f}F_0''' + (f_0+g_0)F_0'' + (F_0+G_0)f_0'' - \frac{2n}{n+1}(2f_0' - \gamma)F_0' - \frac{2n}{n+1}(f_0'G_0' + g_0'F_0')$$
$$-\frac{2n}{n+1}\frac{\sigma_{nf}/\sigma_f}{\rho_{nf}/\rho_f}MF_0' = 0, \tag{33}$$

$$\frac{\mu_{nf}/\mu_f}{\rho_{nf}/\rho_f}G_0''' + (f_0+g_0)G_0'' + (F_0+G_0)g_0'' - \frac{2n}{n+1}(2g_0' - \gamma)G_0' - \frac{2n}{n+1}(f_0'G_0' + g_0'F_0')$$
$$-\frac{2n}{n+1}\frac{\sigma_{nf}/\sigma_f}{\rho_{nf}/\rho_f}MG_0' = 0, \tag{34}$$

$$\frac{1}{\Pr\left(\left(\rho C_p\right)_{nf}/\left(\rho C_p\right)_f\right)}\left(\frac{k_{nf}}{k_f} + \frac{4}{3}R\right)H_0'' + (F_0+G_0)\theta_0'$$
$$+ (f_0+g_0)H_0' + \frac{2\gamma}{n+1}H_0 = 0, \tag{35}$$

$$F_0(0) = 0,\ G_0(0) = 0,\ H_0(0) = 0,\ F_0'(0) = 0,\ G_0'(0) = 0,$$
$$F_0'(\eta) \to 0,\ G_0'(\eta) \to 0,\ H_0(\eta) \to 0,\ \text{as } \eta \to \infty. \tag{36}$$

According to Harris et al. [54], a relaxing condition $F_0''(0) = 1$ is used in place of the boundary condition $F_0'(\eta) \to 0$ as $\eta \to \infty$ to ensure that the nonzero smallest eigenvalues are successfully generated.

5. Results and discussion

The primary instrument for the data analysis is the bvp4c (Matlab) function. To examine the flow and heat transfer characteristics, similarity differential equations as stated in Eqs. (13)–(15) are calculated together with the condition (16). The identification of the non-unique solutions that satisfy all the far field boundary requirements is conducted with $\eta_\infty = 15$. The model when $\phi = M = S = R = 0$, $\lambda = -1$ and $n = 1$ is solved and displayed in Table 3 for the current method's verification. The parameters in this research are determined within the bounds of $0.01 \leqslant \phi \leqslant 0.015$, $50 < R \leqslant 100$, $0 < M \leqslant 1$, $1 \leqslant n \leqslant 3$ and $\lambda_c \leqslant \lambda \leqslant -3$. Following Ramzan et al. [29], the Prandtl number $\Pr = 1000$ is chosen because the Prandtl number for a lubricant like vacuum pump oil is within $600 \leqslant \Pr \leqslant 6000$. These values are employed in accordance with the published works and the incidence of the solutions.

The critical value λ_c or sometimes referred to as a separation point, is the intersection of the solutions where no boundary solution(s) is possible when $\lambda < \lambda_c$. In the situation where the boundary layer begins to separate ($\lambda < \lambda_c$), the flow characteristics cannot be observed and analyzed using Eqs. (13)–(16). Besides, the authors also highlight the parameters which are beneficial in extending the boundary layer separation process (by extending λ_c) as presented in Figs. 2-8. The list of critical values with the increment of the parameters is displayed in Table 4. The expansion of critical value is seen by increasing the volumetric concentration of the magnetite nanoparticle and magnetic parameter. Unexpectedly, the nonlinear parameter based on power-law velocity ($n > 1$) fails to prevent the separation process as compared to the linear shrinking velocity ($n = 1$) while the thermal radiation is not changing the boundary layer separation. Based on the presented figures in this section, the duality of solutions is detected which leads to the conduct of stability analysis. By considering Eqs. (33)-(35) with the relaxing conditions modified from the Eq. (36), the stability of the dual solutions is performed using the bvp4c solver and the results are displayed in Table 5. The smallest eigenvalues are calculated within the range of $-3.19 \leqslant \lambda \leqslant -3.1984(\lambda_c)$ where $M = 0$, $\phi = 0.01$, $R = 100$,

Table 3 Model validation when $\phi = M = S = R = 0$, $\lambda = -1$ and $n = 1$.

Pr	Wang [55]	Khan and Pop [56]	Rashidi et al. [57]	Mabood et al. [58]	Present
0.7	0.4539	0.4539	–	0.4539	0.453932427
2	0.91136	–	0.91136	–	0.911357644
7	1.8954	1.8954	1.8954	1.8954	1.895403243
20	3.3539	3.3539	–	3.3539	3.353904128
70	6.4622	6.4621	–	6.4622	6.462199534

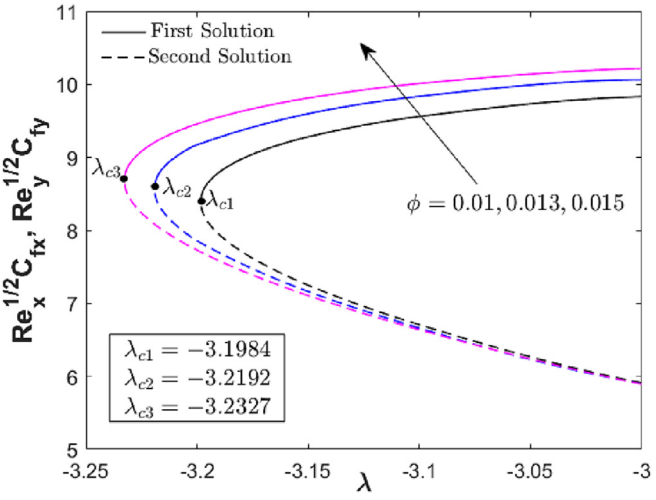

Fig. 2 $Re_x^{1/2}C_{fx}$ and $Re_y^{1/2}C_{fy}$ for various ϕ (nanoparticle concentration).

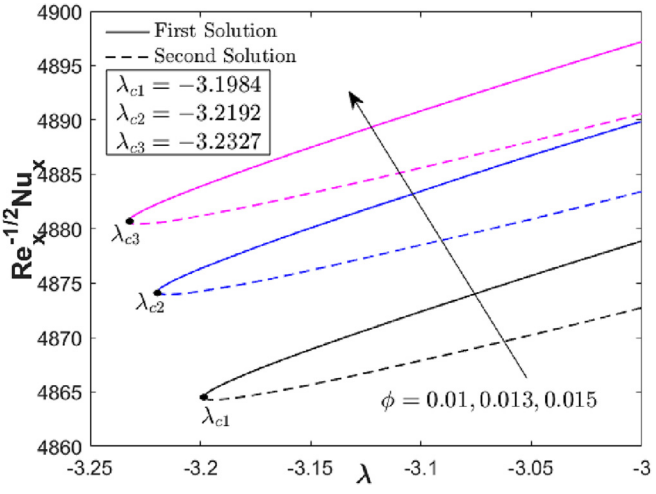

Fig. 3 $Re_x^{-1/2}Nu_x$ for various ϕ (nanoparticle concentration).

$S = 5$ and $n = 1$. It is clear that the first solution with positive smallest eigenvalues is more stable than the second solution (negative eigenvalues). Hence, for the flow and thermal behaviors, only the first solution is highlighted in the discussion section while the second solution (unstable) usually has the opposite trend of behaviors as compared to the first solution.

Since the nanofluid motion is axisymmetric with same shrinking velocities (λ), the values of the skin friction coefficients in $x-$ and $y-$ directions are identical as shown in Fig. 2. An increase in ϕ contributes to the enlargement of λ_c where $\lambda_{c1} = -3.1984$ ($\phi = 0.01$), $\lambda_{c2} = -3.2192$ ($\phi = 0.013$) and $\lambda_{c3} = -3.2327$ ($\phi = 0.015$). In addition, $Re_x^{1/2}C_{fx}$,

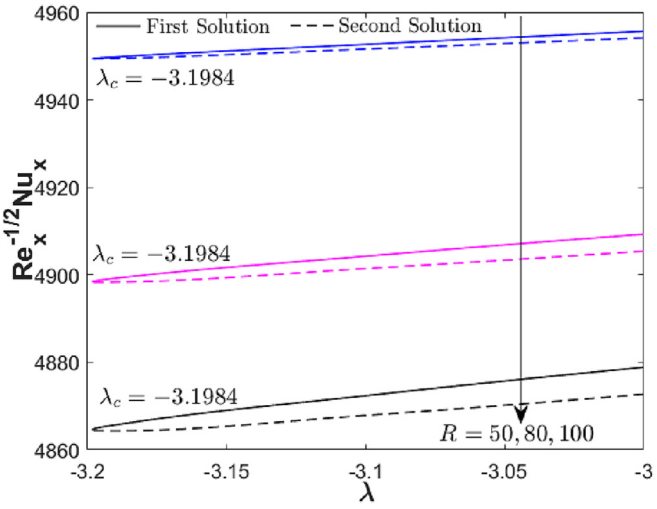

Fig. 4 $Re_x^{-1/2}Nu_x$ for various R (radiation parameter).

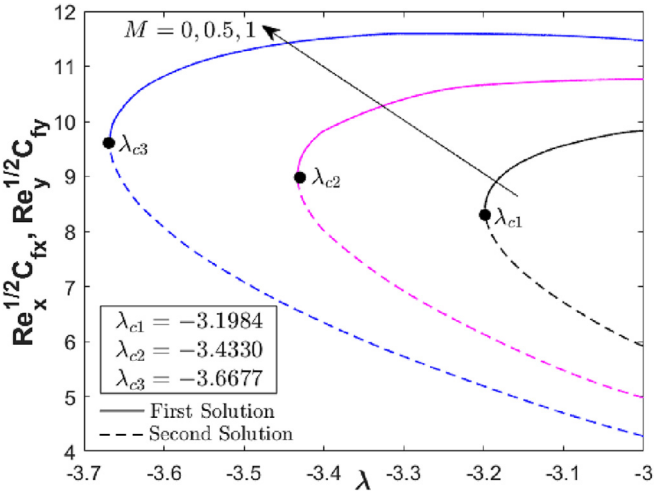

Fig. 5 $Re_x^{1/2}C_{fx}$ and $Re_y^{1/2}C_{fy}$ for various M (magnetic parameter).

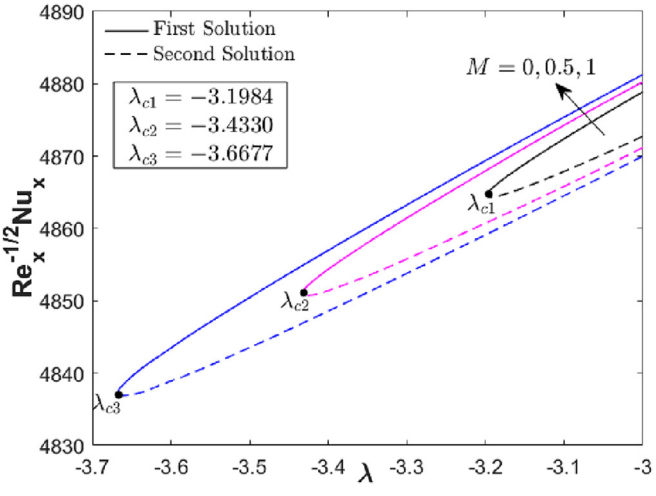

Fig. 6 $Re_x^{-1/2}Nu_x$ for various M (magnetic parameter).

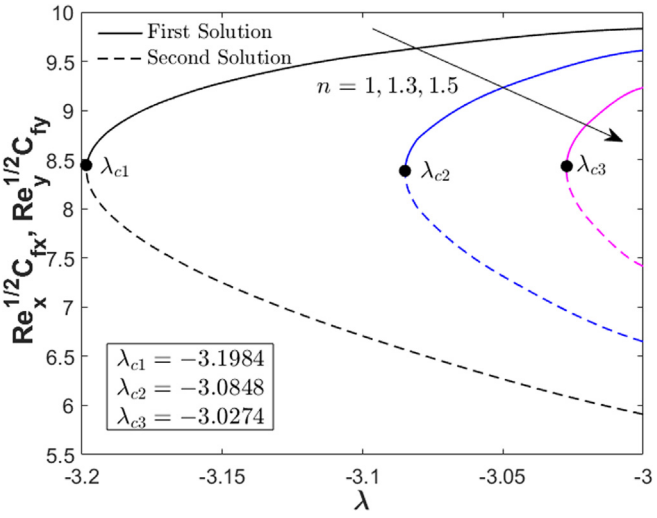

Fig. 7 $Re_x^{1/2}C_{fx}$ and $Re_y^{1/2}C_{fy}$ for various n (power exponent/nonlinear parameter).

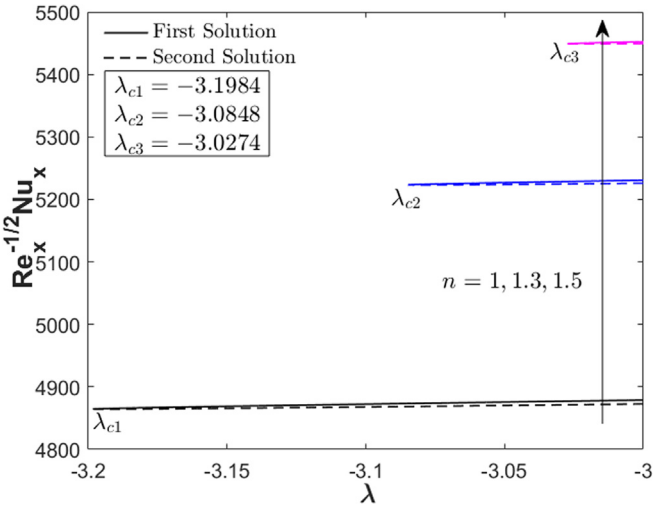

Fig. 8 $Re_x^{-1/2}Nu_x$ for various n (power exponent/nonlinear parameter).

Table 4 Critical values λ_c for various parameters.

ϕ	R	M	n	λ_c
0.01	100	0	1	−3.1984
0.013				−3.2192
0.015				−3.2327
0.01	80			−3.1984
	50			−3.1984
	100	0.5		−3.4330
		1		−3.6677
		0	1.3	−3.0848
			1.5	−3.0274

Table 5 Smallest eigenvalues of the dual solutions using stability analysis.

λ	Smallest Eigenvalues	
	First Solution	Second Solution
−3.19	0.387	−0.3763
−3.195	0.2459	−0.2416
−3.197	0.1584	−0.1566
−3.198	0.0868	−0.0862
−3.1984	0.0235	−0.0235

$Re_y^{1/2}C_{fy}$ and $Re_x^{-1/2}Nu_x$ for the first solution also enhances with the increment of ϕ. Theoretically, the presence and addition of nanoparticles will enhance the kinetic energy of the fluid particles, yet, increasing the skin friction coefficients while delay the separation of boundary layer flow as seen in Fig. 2. Besides, this energy also activates the heat transmission from fluid to the wall surface, and simultaneously increases the heat transfer rate as clearly displayed in Fig. 3.

Fig. 4 shows the effect of the radiation parameter on the heat transfer rate distribution. The energy transmission mechanism from thermal radiation is not involving in the change of laminar-turbulent flow process, hence, the critical

value remains unaltered as this parameter increases. Further observation can be seen through the the thermal progress, where it is reduced when the radiation parameter rises. Generally, the working fluid's thermal performance was improved by the radiation process through the conversion of thermal energy [59]. However, in this work, the use of shrinking sheets may have an impact on how well the nanofluids' heat transport by degrading energy transmission. Further, magnetite is one of the suitable magnetic composites that can be magnetized and, relates to the magnetohydrodynamics (MHD) theory [18]. The boundary layer separation is frequently delayed by the magnetic effect and this proven by Figs. 5 and 6 where the critical values significantly enlarges with the increment of the magnetic parameter such that $\lambda_{c1} = -3.1984$ $(M = 0)$, $\lambda_{c2} = -3.4330$ $(M = 0.5)$ and $\lambda_{c3} = -3.6677$ $(M = 1)$. Basically, the magnetic field created a drag/resistance Lorentz force that opposes the velocity of the fluid and consequently, delays the separation of the boundary layer.

Figs. 7 and 8 exhibit the effect of power exponent/nonlinear parameter (based on the power law velocity of the shrinking surface) on the distributions of $Re_x^{1/2}C_{fx}$, $Re_y^{1/2}C_{fy}$ and $Re_x^{-1/2}Nu_x$. As stated in Table 4, the critical value is diminished as the value of n increases which shows that the shrinking surface with nonlinear velocity $(n > 1)$ accelerates the boundary layer separation as compared to the linear shrinking surface $(n = 1)$. However, the thermal rate when considering $n > 1$ is significantly higher than the case of $n = 1$ which shows the efficiency of using nonlinear shrinking surface for the enhancement of heat transfer. Figs. 9 and 10 respectively display the profiles of velocity and temperature with various n. All the profiles are fulfilled the boundary conditions asymptotically which implies the correctness of the mathematical computation via the bvp4c solver. The findings show that the nanofluid velocity depreciates while the temperature shows reverse result.

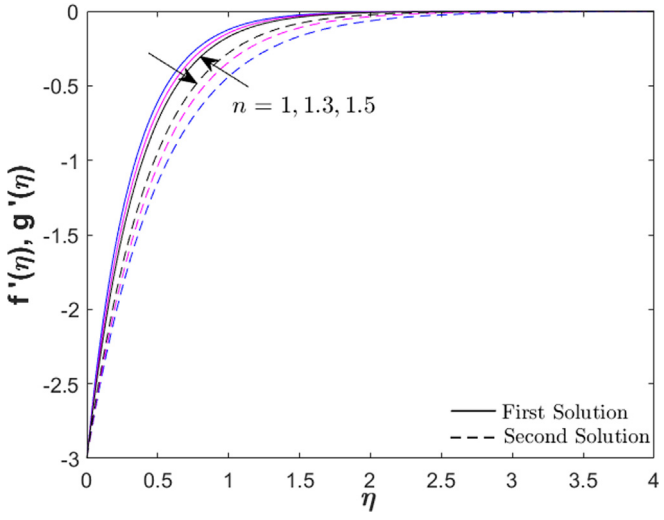

Fig. 9 Velocity profile for various n (power exponent/nonlinear parameter).

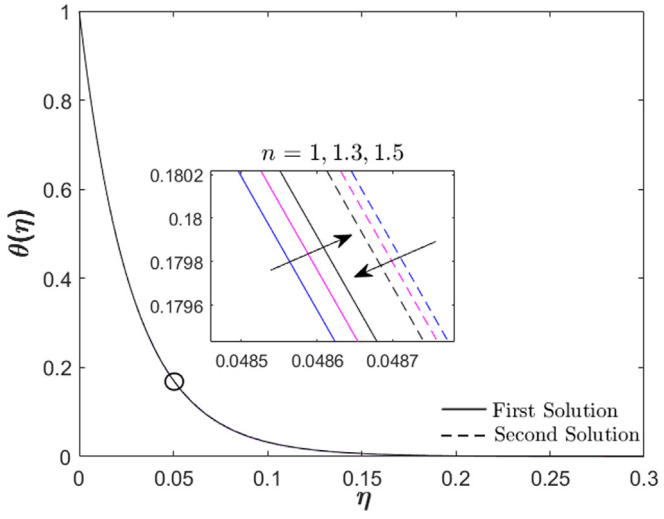

Fig. 10 Temperature profile for various n (power exponent/nonlinear parameter).

6. Conclusions

The research questions presented in the Introduction section serve as the foundation for the conclusions. For the validation part of the model and method, a few of numerical values was compared to the published values to assess the results' correctness. Following is the list of the conclusions:

- The suction parameter is requirable in inducing the multiple solutions for the magnetite-VPO bidirectional flow under simultaneous effects of the shrinking surface, MHD and radiation parameters.
- Within the defined ranges of the physical parameters, two solutions are found.
- The first solution which has positive smallest eigenvalues, represents physical behavior. The second solution, on the other hand, exhibits contradictory flow and temperature behaviors and has negative lowest eigenvalues, indicating an unstable solution.
- The developing factors which delay the flow separation are volumetric concentrations of the nanoparticles and magnetic parameter. Meanwhile, the thermal radiation is not aiding/opposing the boundary layer separation.
- The enhancement of volumetric concentrations of the nanoparticles and magnetic parameter also develops the skin friction coefficients and thermal rate of the tested nanofluid. However, the radiation parameter significantly reduces the heat transfer progression.
- The linear shrinking surface can extend the critical value, but, for thermal enhancement, the nonlinear shrinking surface can significantly develop the thermal rate better than the linear shrinking surface.

Declaration of Competing Interest

The authors declare that they have no known competing financial interests or personal relationships that could have appeared to influence the work reported in this paper.

Acknowledgments

We acknowledge the research supports from Babeş-Bolyai University and Universiti Teknikal Malaysia Melaka. The work of Ioan Pop has been supported from the grant PN-III-P4-PCE-2021-0993, UEFISCDI, Romania. The authors also wish to express their thank to the very competent Reviewers for the valuable comments and suggestions.

References

[1] J.C.A. Maxwell, treatise on electricity and magnetism, Oxford Clarendon Press, 1873,, pp. 360–366.
[2] P. Keblinski, S.R. Phillpot, S.U.S. Choi, J.A. Eastman, Mechanisms of heat flow in suspensions of nano-sized particles (nanofluids), Int J Heat Mass Transfer. 45 (2002) 855–863.
[3] Choi SUS, Eastman JA. Enhancing thermal conductivity of fluids with nanoparticles. Proc 1995 ASME Int Mech Eng Congr Expo, San Francisco, USA. 1995;99–105.
[4] A. Kasaeian, R. Daneshazarian, O. Mahian, L. Kolsi, A.J. Chamkha, S. Wongwises, I. Pop, Nanofluid flow and heat transfer in porous media: a review of the latest developments, Int J Heat Mass Transfer. 107 (2017) 778–791.
[5] E. Ebrahimnia-Bajestan, M.C. Moghadam, H. Niazmand, W. Daungthongsuk, S. Wongwises, Experimental and numerical investigation of nanofluids heat transfer characteristics for application in solar heat exchangers, Int J Heat Mass Transfer. 92 (2016) 1041–1052.
[6] N.A. Sidik, M.N. Yazid, R. Mamat, A review on the application of nanofluids in vehicle engine cooling system, Int Commun Heat Mass Transfer. 68 (2015) 85–90.
[7] O. Mahian, A. Kianifar, S.A. Kalogirou, I. Pop, S.A. Wongwises, A review of the applications of nanofluids in solar energy, Int J Heat Mass Transfer. 57 (2013) 582–594.
[8] Z. Haddad, H.F. Oztop, E. Abu-Nada, A. Mataoui, A review on natural convective heat transfer of nanofluids, Renew Sust Energy Rev. 16 (2012) 5363–5378.
[9] L. Blaney, Magnetite (Fe_3O_4): properties, synthesis, and applications, Lehigh Rev. 15 (2007).
[10] I. Sharifi, H. Shokrollahi, S. Amiri, Ferrite-based magnetic nanofluids used in hyperthermia applications, J Magn Magn Mater 324 (6) (2012) 903–915.
[11] M. Bahiraei, M. Hangi, Flow and heat transfer characteristics of magnetic nanofluids: a review, J Magn Magn Mater 374 (2015) 125–138.
[12] L.G. Petrescu, M.C. Petrescu, V. Ioniță, E. Cazacu, C.D. Constantinescu, Magnetic Properties of Manganese-Zinc Soft Ferrite Ceramic for High Frequency Applications, Mater. 12 (19) (2019) 3173.
[13] E.H. Aly, A. Ebaid, Exact analytical solution for suction and injection flow with thermal enhancement of five nanofluids over an isothermal stretching sheet with effect of the slip model: a comparative study, Abstr Appl Anal. 721578 (2013) 1–14.
[14] M.G. Reddy, Influence of magnetohydrodynamic and thermal radiation boundary layer flow of a nanofluid past a stretching sheet, J Sci Res. 6 (2014) 257–272.
[15] Z. Abbas, R. Perveen, M. Sheikh, I. Pop, Thermophoretic diffusion and nonlinear radiative heat transfer due to a contracting cylinder in a nanofluid with generalized slip condition, Results Phys. 6 (2016) 1080–1087.
[16] J. Buongiorno, Convective transport in nanofluids, J Heat Transfer. 128 (2006) 240–250.
[17] R.K. Tiwari, M.K. Das, Heat transfer augmentation in a two-sided lid-driven differentially heated square cavity utilizing nanofluids, Int J Heat Mass Transfer. 50 (9–10) (2007) 2002–2018.
[18] R. Jusoh, R. Nazar, I. Pop, Magnetohydrodynamic rotating flow and heat transfer of ferrofluid due to an exponentially permeable stretching/shrinking sheet, J Magn Magn Mater 465 (2018) 365–374.
[19] N. Ahmed, A. Tassaddiq, R. Alabdan, U. Khan, S. Noor, S.T. Mohyud-Din, I. Khan, Applications of nanofluids for the thermal enhancement in radiative and dissipative flow over a wedge, Appl Sci. 9 (10) (2019) 1976.
[20] T. Hayat, M. Rashid, A. Alsaedi, Three dimensional radiative flow of magnetite-nanofluid with homogeneous-heterogeneous reactions, Results Phys. 8 (2018) 268–275.
[21] M.K. Mohamed, N.A. Ismail, N. Hashim, N.M. Shah, M.Z. Salleh, MHD slip flow and heat transfer on stagnation point of a magnetite (Fe_3O_4) ferrofluid towards a stretching sheet with Newtonian heating, CFD Lett. 11 (1) (2019) 17–27.
[22] S. Areekara, F. Mabood, A.S. Sabu, A. Mathew, I.A. Badruddin, Dynamics of water conveying single-wall carbon nanotubes and magnetite nanoparticles subject to induced

magnetic field: A bioconvective model for theranostic applications, Int Comm Heat Mass Transfer 126 (2021) 105484.
[23] N.S. Khashi'ie, N.S. Wahid, N.M. Arifin, I. Pop, Insight into three-dimensional flow of three different dynamics of nanofluids subject to thermal radiation: The case of water–cobalt ferrite, water–manganese–zinc ferrite, and water–magnetite, Heat Transfer 51 (5) (2022) 4434–4450.
[24] Adio SA, Alo TA, Olagoke RO, Olalere AE, Veeredhi VR, Ewim DR. Thermohydraulic and entropy characteristics of Al_2O_3-water nanofluid in a ribbed interrupted microchannel heat exchanger. Heat Transfer 202;50(3):1951-84.
[25] A.K. Pandey, M. Kumar, Natural convection and thermal radiation influence on nanofluid flow over a stretching cylinder in a porous medium with viscous dissipation, Alexandria Eng. J. 56 (1) (2017) 55–62.
[26] N.S. Khashi'ie, N.M. Arifin, I. Pop, R. Nazar, E.H. Hafidzuddin, N. Wahi, Flow and heat transfer past a permeable power-law deformable plate with orthogonal shear in a hybrid nanofluid, Alexandria Eng. J. 59 (3) (2020) 1869–1879.
[27] Khashi'ie NS, Arifin NM, Hafidzuddin EH, Wahi N. Dual stratified nanofluid flow past a permeable shrinking/stretching sheet using a non-Fourier energy model. Appl. Sci. 2019;9 (10):2124.
[28] N.S. Khashi'ie, N.M. Arifin, N.C. Rosca, A.V. Rosca, I. Pop, Three-dimensional flow of radiative hybrid nanofluid past a permeable stretching/shrinking sheet with homogeneous-heterogeneous reaction, Int J Numer Methods Heat Fluid Flow. 32 (2) (2022) 568–588.
[29] M. Ramzan, Z. Shah, P. Kumam, W. Khan, W. Watthayu, W. Kumam, Bidirectional flow of MHD nanofluid with Hall current and Cattaneo-Christove heat flux toward the stretching surface, Plos One 17 (4) (2022) e0264208.
[30] H. Upreti, A.K. Pandey, M. Kumar, Assessment of entropy generation and heat transfer in three-dimensional hybrid nanofluids flow due to convective surface and base fluids, J. Porous Media 24 (3) (2021).
[31] A.K. Pandey, H. Upreti, Mixed convective flow of Ag–H_2O magnetic nanofluid over a curved surface with volumetric heat generation and temperature-dependent viscosity, Heat Transfer 50 (7) (2021) 7251–7270.
[32] N.A. Shah, I.L. Animasaun, J.D. Chung, A. Wakif, F.I. Alao, C.S. Raju, Significance of nanoparticle's radius, heat flux due to concentration gradient, and mass flux due to temperature gradient: the case of water conveying copper nanoparticles, Sci. Rep. 11 (1) (2021) 1.
[33] G. Sowmya, B.J. Gireesha, I.L. Animasaun, N.A. Shah, Significance of buoyancy and Lorentz forces on water-conveying iron (III) oxide and silver nanoparticles in a rectangular cavity mounted with two heated fins: heat transfer analysis, J. Therm. Anal. Calorim. 144 (2021) 2369–2384.
[34] N.S. Khashi'ie, I. Waini, N.S. Wahid, N.M. Arifin, I. Pop, Radiative Hybrid Ferrofluid Flow Over a Permeable Shrinking Sheet in a Three-Dimensional System, CFD Lett. 14 (11) (2022) 9–21.
[35] Wahid NS, Arifin NM, Khashi'ie NS, Pop I, Bachok N, Hafidzuddin EH. Mixed Convection Magnetic Nanofluid Flow past a Rotating Vertical Porous Cone. J. Appl. Fluid Mech. 2022;15(4):1207-20.
[36] I. Khan, New idea of Atangana and Baleanu fractional derivatives to human blood flow in nanofluids. Chaos: Interdisciplinary, J. Nonlinear Sci. 29 (1) (2019) 013121.
[37] I. Khan, Ramped heating in CNTS fractional nanofluids. Case Studies, Therm. Eng. (2023) 102836.
[38] H.B. Lanjwani, M.S. Chandio, M.I. Anwar, S.A. Shehzad, M. Izadi, Mhd laminar boundary layer flow of radiative fe-casson nanofluid: stability analysis of dual solutions, Chinese J. Phys. 76 (2022) 172–186.
[39] H.B. Lanjwani, M.S. Chandio, M.I. Anwar, S.A. Shehzad, M. Izadi, Dual solutions of time-dependent magnetohydrodynamic stagnation point boundary layer micropolar nanofluid flow over shrinking/stretching surface, Appl. Math. Mech. 42 (7) (2021) 1013–1028.
[40] I. Khan, A.M. Alqahtani, A. Khan, D. Khan, A.H. Ganie, G. Ali, New results of fractal fractional model of drilling nanoliquids with clay nanoparticles, Fractals 30 (01) (2022) 2250024.
[41] S.K. Das, S.U.S. Choi, W. Yu, Y. Pradeep, Nanofluids: Science and Technology, Wiley, New Jersey, 2008.
[42] D.A. Nield, A. Bejan, Convection in Porous Media, 5th ed., Springer, New York, 2017.
[43] A. Shenoy, M. Sheremet, I. Pop, Convective Flow and Heat Transfer from Wavy Surfaces: Viscous Fluids, Porous Media and Nanofluids, CRC Press, Taylor & Francis Group, New York, 2016.
[44] J.H. Merkin, I. Pop, Y.Y. Lok, T. Grosan, Similarity Solutions for the Boundary Layer Flow and Heat Transfer of Viscous Fluids, Nanofluids, Porous Media, and Micropolar Fluids, Elsevier, Oxford, UK, 2021.
[45] J.A. Shercliff, A Textbook of Magnetohydrodynamics, Pergamon Press, New York, 1965.
[46] R. Cortell, Heat and fluid flow due to non-linearly stretching surfaces, Appl. Math. Comput. 217 (2011) 7564–7572.
[47] S. Rosseland, Astrophysik und Atom-Theoretische Grundlagen, Springer, Berlin/Heidelberg, Germany, 1931.
[48] M. Govindaraju, N.V. Ganesh, B. Ganga, A.A. Hakeem, Entropy generation analysis of magneto hydrodynamic flow of a nanofluid over a stretching sheet, J. Egypt Math. Soc. 23 (2) (2015) 429–434.
[49] M. Miklavčič, C. Wang, Viscous flow due to a shrinking sheet, Quarterly Appl. Math. 64 (2) (2006) 283–290.
[50] I. Waini, A. Ishak, I. Pop, Multiple solutions of the unsteady hybrid nanofluid flow over a rotating disk with stability analysis, Eur. J. Mech. B Fluids 94 (2022) 121–127.
[51] N.S. Khashi'ie, I. Waini, N.A. Zainal, K.B. Hamzah, N.M. Arifin, I. Pop, Multiple Solutions and Stability Analysis of Magnetic Hybrid Nanofluid Flow Over a Rotating Disk with Heat Generation. J. Adv. Res. Fluid Mech, Therm. Sci. 102 (1) (2023) 59–72.
[52] J.H. Merkin, On dual solutions occurring in mixed convection in a porous medium, J. Eng. Math. 20 (1986) 171–179.
[53] P.D. Weidman, D.G. Kubitschek, A.M.J. Davis, The effect of transpiration on self similar boundary layer flow over moving surfaces, Int. J. Eng. Sci. 44 (2006) 730–737.
[54] S.D. Harris, D.B. Ingham, I. Pop, Mixed convection boundary-layer flow near the stagnation point on a vertical surface in a porous medium: Brinkman model with slip, Transp. Porous Media. 77 (2009) 267–285.
[55] C.Y. Wang, Free convection on a vertical stretching surface, ZAMM-J. Appl. Math. Mech. 69 (11) (1989) 418–420.
[56] W.A. Khan, I. Pop, Boundary-layer flow of a nanofluid past a stretching sheet, Int. J. Heat Mass Transfer 53 (11–12) (2010) 2477–2483.
[57] M.M. Rashidi, N.V. Ganesh, A.A. Hakeem, B. Ganga, Buoyancy effect on MHD flow of nanofluid over a stretching sheet in the presence of thermal radiation, J. Mol. Liq. 198 (2014) 234–238.
[58] F. Mabood, W.A. Khan, A.M. Ismail, MHD boundary layer flow and heat transfer of nanofluids over a nonlinear stretching sheet: a numerical study, J. Mag. Magn. Mater. 374 (2015) 569–576.
[59] N.A. Zainal, R. Nazar, K. Naganthran, I. Pop, MHD flow and heat transfer of hybrid nanofluid over a permeable moving surface in the presence of thermal radiation, Int. J. Numer. Methods Heat Fluid Flow 31 (3) (2021) 858–879.